More than marine heatwaves: A new regime of heat, acidity, and low oxygen compound extreme events in the Gulf of Alaska

Claudine Hauri[1*], Rémi Pagès[1], Katherine Hedstrom[2], Scott C. Doney[3], Sam Dupont[4], Bridget Ferriss[5], and Malte F. Stuecker[6]

[1] International Arctic Research Center, University of Alaska Fairbanks, Fairbanks, AK, USA

[2]College of Fisheries and Ocean Sciences, University of Alaska Fairbanks, Fairbanks, AK, USA

[3]Department of Environmental Sciences, University of Virginia, Charlottesville, VA, USA

[4] Department of Biological and Environmental Sciences, University of Gothenburg, Fiskebäckskil, Sweden

[5] Resource Ecology and Fisheries Management Division, Alaska Fisheries Science Center, NOAA Fisheries, Seattle, WA, USA

[6]Department of Oceanography and International Pacific Research Center, School of Ocean and Earth Science and Technology, University of Hawai‘i at Mānoa, Honolulu, HI, USA

Corresponding author: Claudine Hauri (chauri@alaska.edu)

Key Points:

- 20 % of the bottom water was exposed to quadruple heat, positive $[H^+]$, negative Ω_{arag}, and negative $[O_2]$ compound extreme events during 2018-2020 marine heat wave

· Interaction of marine heat waves and local natural variability of deep-water intrusion triggered quadruple compound extreme events on shelf seafloor

· New Gulf of Alaska Downwelling Index presented as indicator for environmental conditions on continental shelf

Abstract

Recent marine heatwaves in the Gulf of Alaska have had devastating and lasting impacts on species from various trophic levels. As a result of climate change, total heat exposure in the upper ocean has become longer, more intense, more frequent, and more likely to happen at the same time as other environmental extremes. The combination of multiple environmental extremes can exacerbate the response of sensitive marine organisms. Our hindcast simulation provides the first indication that more than 20 % of the bottom water of the Gulf of Alaska continental shelf was exposed to quadruple heat, positive $[H^+]$, negative Ω_{arag}, and negative $[O_2]$ compound extreme events during the 2018-2020 marine heat wave. Natural intrusion of deep and acidified water combined with the marine heat wave triggered the first occurrence of these events in 2019. During the 2013-2016 marine heat wave, surface waters were already exposed to widespread marine heat and positive $[H^+]$ compound extreme events due to the temperature effect on the $[H^+]$. We introduce a new Gulf of Alaska Downwelling Index (GOADI) with short-term predictive skill, which can serve as indicator of past and near-future positive $[H^+]$, negative Ω_{arag}, and negative $[O_2]$ compound extreme events on the shelf. Our results suggest that the marine heat waves may have not been the sole environmental stressor that led to the observed ecosystem impacts and warrant a closer look at existing *in situ* inorganic carbon and other environmental data in combination with biological observations and model output.

Plain Language Summary

The Gulf of Alaska supports a rich ocean ecosystem and valuable fisheries. Climate change and ocean acidification threaten to disrupt marine life in the region from plankton to fish, marine mammals, and sea birds. The gradual build-up of these environmental pressures can be exacerbated further by short-term extreme events, such as marine heat waves, that can temporarily push ocean conditions beyond physiological and ecological thresholds for some organisms. The problem is worsened by the co-occurrence of extreme events for multiple factors, for example heat and acidity. Our analysis using a regional ocean model indicates that such compound extreme events have become more frequent and intense with time in the Gulf of Alaska, raising concerns for vulnerable parts of the ecosystem. Improvements in model forecasts and observing systems may help by providing advanced warning of compound extreme events and be useful to fisheries and marine resource managers as they develop climate adaptation strategies.

1 Introduction

Climate change and ocean acidification are gradually altering the environmental properties of the ocean. As these long-term changes in temperature, pH, and oxygen unfold, extreme conditions will happen more often, last longer, and become more intense (Burger et al., 2020; Gruber et al., 2021; Laufkötter et al., 2020; Rodgers et al., 2021). The tendency towards longer and more intense extreme events increases the likelihood that more than one ocean ecosystem driver is simultaneously outside the norm to which organisms have adapted, in close spatial proximity or temporal succession (compound extreme events; Leonard et al., (2014)). A preponderance of evidence shows that compound extreme events with warmer temperature,

higher [H^+], lower [O_2], and/or food shortage will lead to a more severe and harmful biological response than if exposed to just one single stressor (Breitberg et al., 2015; Kroeker et al., 2021; Thomsen et al., 2013). At the same time, abrupt extremes will have different consequences for the adaptation potential of organisms to global changes than evolutionary response to the gradual long-term changes, such as warming, ocean acidification, and deoxygenation (Bell et al., 2021). This is even more complex for subsequent or compound extreme events that can lead to conflicting selection pressures and decrease the genetic diversity and adaptation potential (Gaitán-Espitia et al., 2017).

The Gulf of Alaska marine ecosystem has been exposed to both marine heat waves and ocean acidification extreme events. However, compound extreme events with multiple environmental conditions outside of their natural variability envelope have not been documented yet. Living marine resources from the Gulf of Alaska not only sustain economically important seafood and tourism industries, but they also play a crucial role in the way of life of Indigenous communities. Recent marine heatwaves have triggered devastating and lasting responses at various trophic levels, from primary producers to commercially and subsistence caught fish species in different regions across the Gulf of Alaska marine ecosystem (Barbeaux et al., 2020; Bellquist et al., 2021; Fisheries, 2023; Piatt et al., 2020; Rogers et al., 2021; Suryan et al., 2021; Von Biela et al., 2019; Weitzman et al., 2021). The longest marine heat wave to date, called “the Blob”, occurred between 2013-2016 (Bond et al., 2015; Di Lorenzo & Mantua, 2016; Hobday et al., 2018). This 2013-2016 marine heat wave was followed by the 2018-2020 marine heat wave (Amaya et al., 2020). The 2013-2016 marine heat wave was initiated by a strong atmospheric ridge over the northeast Pacific in the winter of 2013/2014 that weakened the Aleutian Low and surface winds and caused sea surface temperature changes that project on the Pacific Decadal

Oscillation (PDO) pattern (Bond et al., 2015). A combination of reduced Ekman transport of cold water from the north, decreased upper ocean mixing, and weakened surface heat loss led to a warmer surface ocean. The 2018-2020 marine heat wave (Amaya et al., 2020; Barkhordarian et al., 2022) was primarily driven by a weak North Pacific High, which induced weak surface winds and less evaporative cooling. It started in the summer during a highly stratified period, inducing strong temperature anomalies at the surface (Amaya et al., 2020).

Observations and hindcast model output suggest that the Gulf of Alaska ecosystem has also been exposed to ocean acidity extreme events (Bednaršek et al., 2021; Hauri et al., 2021). Evidence of severe dissolution in pteropod shells, which are an indicator species for ocean acidification, were found in the Gulf of Alaska with concomitant unusually acidified conditions (Bednaršek et al., 2021). These ocean acidity extreme events were likely triggered by a combination of increased upwelling of CO_2-rich water in the Alaskan gyre and ocean acidification from rising atmospheric CO_2 (Hauri et al., 2021). The upwelling strength of the gyre is driven by decadal variability of the local wind stress curl that depresses sea surface height and has been described as the Northern Gulf of Alaska Oscillation (NGAO, Hauri et al., (2021); Figure 1).

There is overwhelming evidence that marine ecosystems and their associated services are under threat as a consequence of local (e.g., over-fishing) and global (e.g., heat waves) changes (Cooley et al., 2022). These pressures combine in a unique way at each location and identifying the major ocean stressor or combination of multiple stressors driving the biological response is critical for the implementation of solutions. For example, addressing local effects of ocean acidification would require a combination of global CO_2 mitigation and local adaptation solutions (e.g., management to increase ecosystem resilience; IOC-UNESCO, 2022). However,

attributing observed biological changes over time in an ecosystem to one or multiple stressors is not an easy task (Widdicombe et al., 2023).

Here, we used output from a regional ocean biogeochemical model that simulated the environmental conditions in the Gulf of Alaska from 1993 through 2021 to study the occurrence and drivers of extreme and compound extreme events at the surface and near the shelf seafloor.

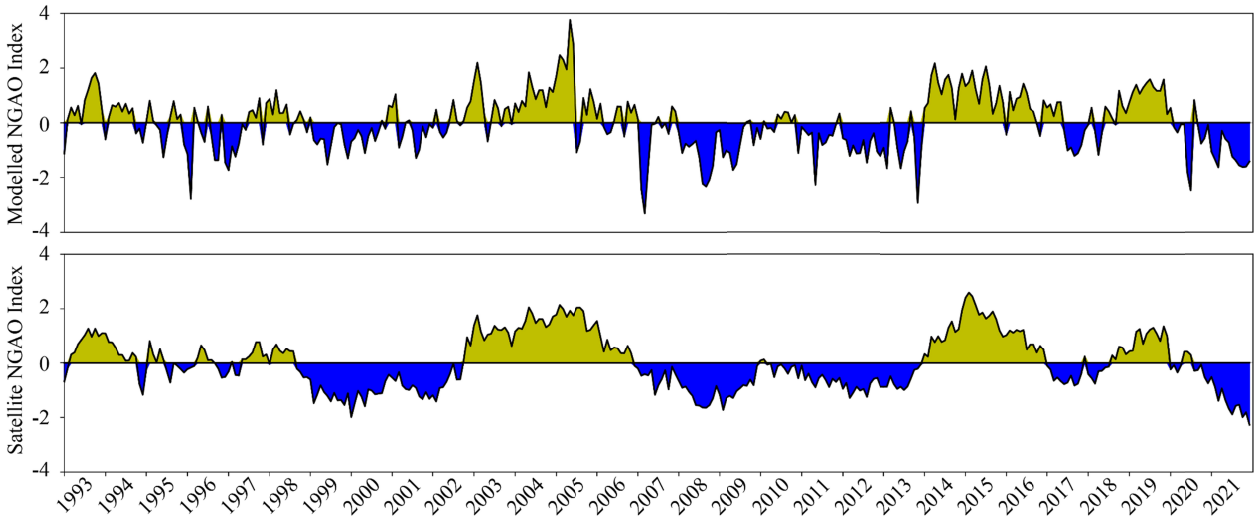

Figure 1. Northern Gulf of Alaska Oscillation Index. Monthly Northern Gulf of Alaska Oscillation (NGAO) index obtained with a) modeled and b) satellite-based (Global Ocean Gridded L4 Sea Surface Heights) sea surface height (SSH). The NGAO index is defined as the first empirical orthogonal function and principal component of SSH variability in our model domain (Hauri et al., 2021). The amount of variance associated with the first EOF of the model is ~ 24%.

2 Materials and Methods

2.1 Model set-up

This study was based on an ocean hindcast simulation (1993 - 2021) with Gulf of Alaska configuration (Figure 2; Hauri et al., (2020, 2021)) of the three-dimensional physical model

Regional Oceanic Modeling System (ROMS, Shchepetkin & McWilliams, (2005)) coupled to the 3PS Carbon, Ocean Biogeochemistry, and Lower Trophic marine ecosystem model (3PS COBALT; (Stock et al., 2014; Van Oostende et al., 2018). The main characteristics of this configuration were the 50 terrain-following depth levels and an eddy-resolving horizontal resolution (4.5 km) that resolves the regional coastal upwelling and downwelling. 3PS-COBALT simulates the cycles of nitrogen, carbon, phosphate, silicate, iron, calcium carbonate, oxygen, and lithogenic material with 36 state variables. More details on the model setup can be found in Hauri et al. (2020) and references therein.

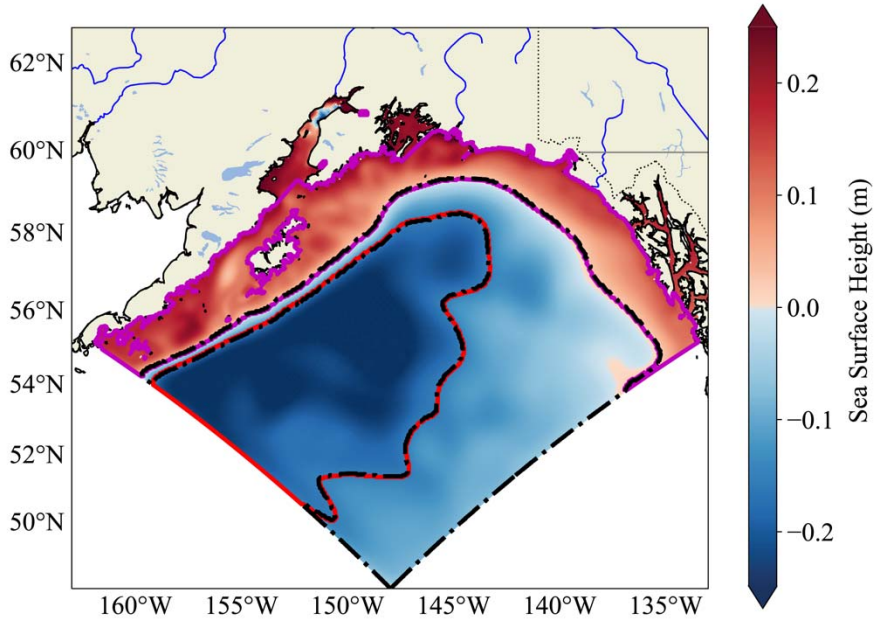

Figure 2. Gulf of Alaska regional biogeochemical model domain. De-seasonalized climatology of the modeled sea surface height (SSH, m) is shown in color. Regions obtained from modeled SSH with a 4 clusters configuration using a classical K-MEANS algorithm (Sculley, 2010) are illustrated by lines. The K-MEANS algorithm was carried out with the scikit-

learn Python package (Pedregosa et al., 2011). Our current analysis focuses on the gyre (red line) and shelf (magenta line) regions.

2.2 Initial and boundary conditions

Physical ocean initial and boundary (daily) conditions (temperature, salinity, and sea surface height) were taken from the Global Ocean Physics Reanalysis (GLORYS; Hamon et al., (2016)) until the end of 2020 and came from Global Ocean Physics Analysis after that. Output from the Japanese 55-year Re-analysis (JRA55-do) version 1.5 (Tsujino et al., 2018) was used as forcing for wind, air-surface temperature, pressure, humidity, precipitation, and radiation at a three-hourly resolution. Data from the NOAA Greenhouse Gas Marine Boundary Layer (Lan et al., 2023) was used as forcing for atmospheric pCO_2. Initial and boundary conditions for nitrate, phosphate, oxygen, and silicate were provided by the World Ocean Atlas 2018 (Boyer et al., 2018). Initial and boundary conditions for iron were provided by a yearly climatology of the GLORYS biogeochemistry reanalysis product (Perruche, 2019). The iron atmospheric soluble deposition was derived from Geophysical Fluid Dynamics Laboratory global products and reduced by 50 % to match the order of magnitude provided by Crusius et al., (2017). Riverine freshwater discharges were the same as in Hauri et al. (2020) derived from Beamer et al. (2016) and Hill et al. (2015). Riverine iron input was set to 100 nM to be more consistent with the value available in Lippiatt et al. (2010). All other river biogeochemical variables are described in Hauri et al. (2020). The chlorophyll to carbon ratio of the different phytoplankton classes has been updated to better simulate the ecosystem of the Gulf of Alaska (Table 1). A 10-year spin-up was run based on a 4-year (1993 to 1996) simulation repeatedly run in a loop. After 10 years the biogeochemical variables reached an approximate seasonally varying steady-state state.

2.3 Model evaluation

The model has been evaluated with available satellite and in situ observations in previous publications (Hauri et al., 2020, 2021). Evaluation of the current version of the hindcast simulation shows that the model simulates the spatial and temporal variability of satellite observed sea surface temperature reasonably well (Figure 3). Point by point comparison of model output with *in situ* dissolved inorganic carbon (DIC), total alkalinity (TA), and oxygen data from various cruises (Figure 4) shows a relatively high Pearson correlation (> 0.8) with statistically significant p-value (<0.01) and low standard deviation and error for the majority of the data points, suggesting that the model represents the observations reasonably well.

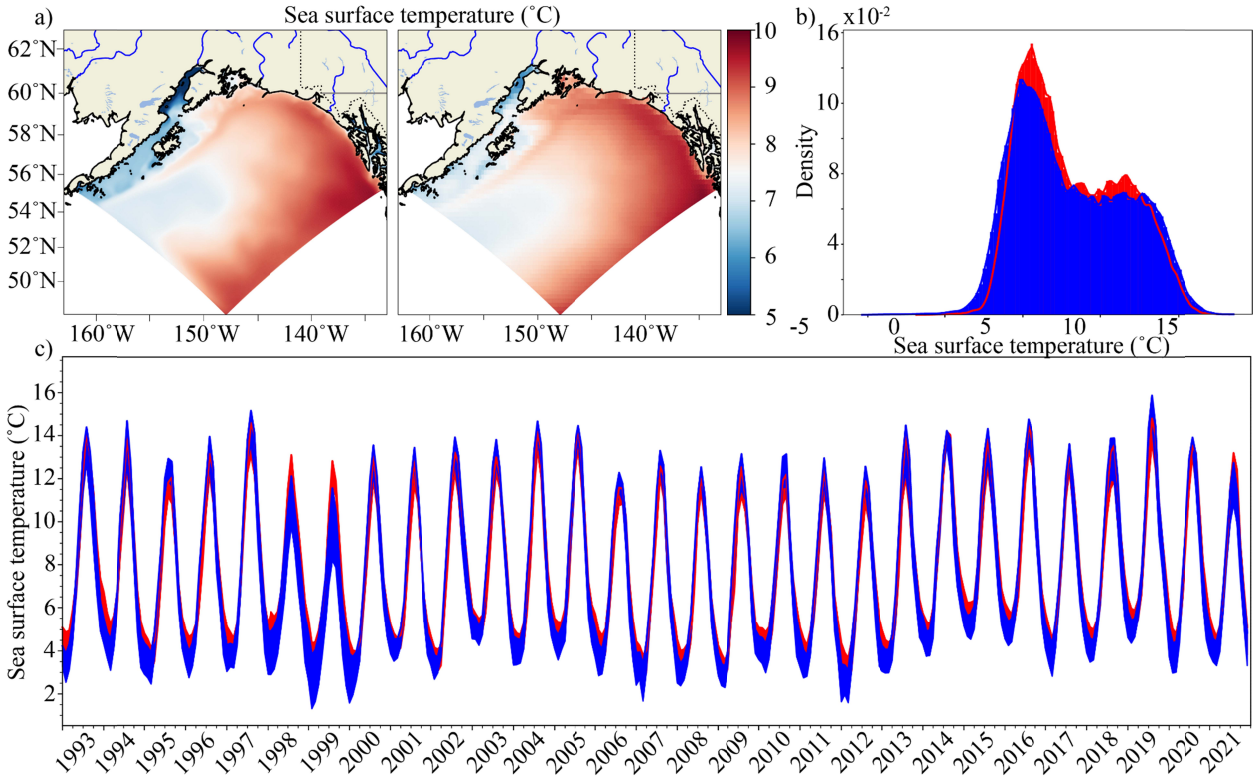

Figure 3. Evaluation of sea surface temperature across the Gulf of Alaska model domain. Maps show the average (a) modeled (left) and satellite observed (right) sea surface temperature

for the time period between 1993 and 2021. Modeled (blue) and satellite observed (red) time-series are illustrated in panel b. Density of probability for modeled (blue) and satellite observed (red) sea surface temperature are shown in panel c.

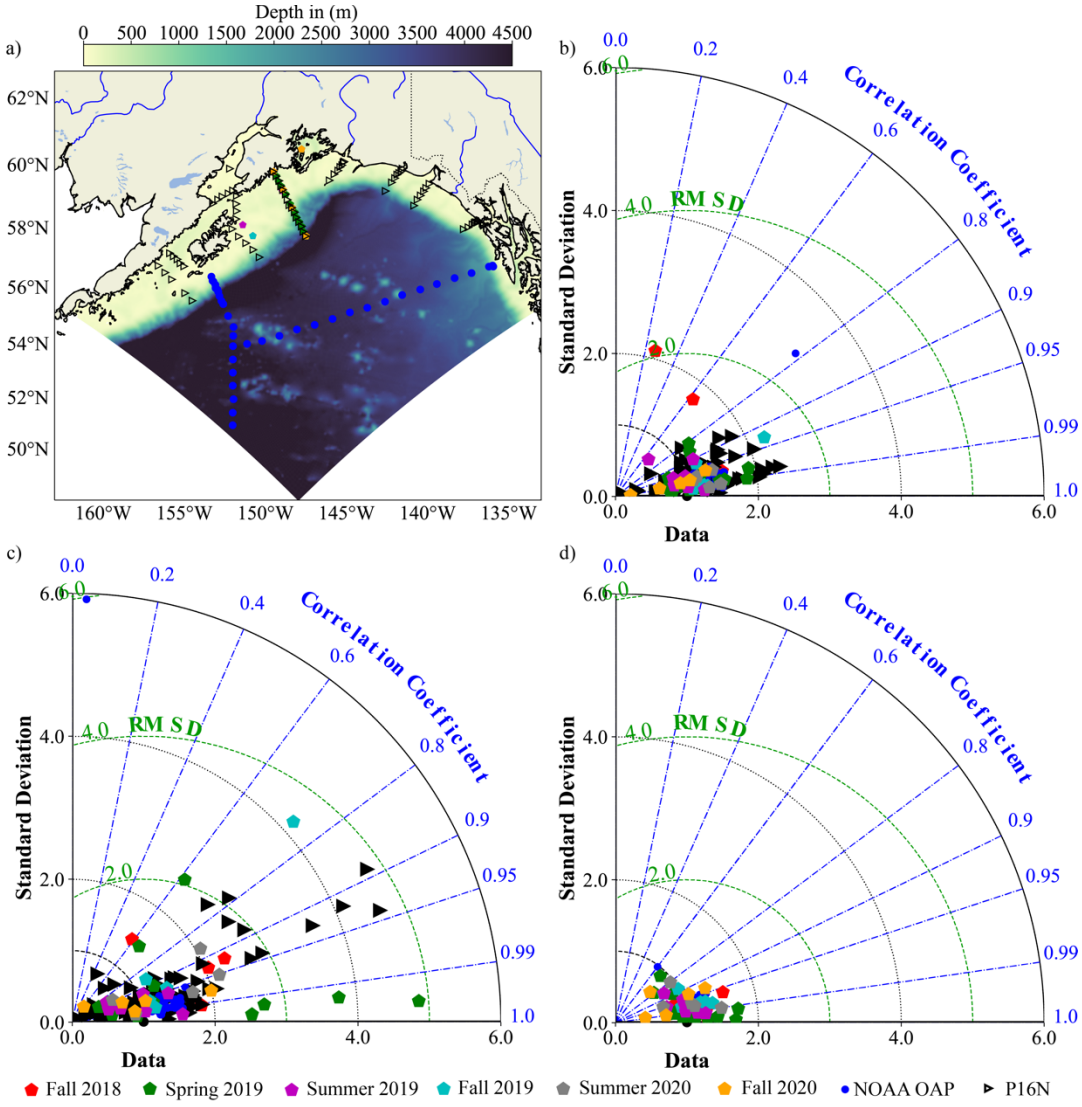

Figure 4. Evaluation of model-simulated dissolved inorganic carbon, total alkalinity and oxygen. Map of stations occupied during several cruises between 2015 and 2020 overlain on water depth (a). Data from the National Oceanographic and Atmospheric Administration ocean

189 acidification cruise in July of 2015 (Cross et al., 2019) are shown by black triangles. The P16N
190 cruise (May - June 2015, Wanninkhof and Denis, 2016) data are illustrated with blue circles. The
191 Long Term Ecological Research (LTER 2018-2020, Hauri & Irving, 2021) cruises data are
192 shown with pentagons of different colors showing different seasons and years. Modeled versus
193 observed b) dissolved inorganic carbon c) total alkalinity, d) oxygen illustrated in the form of
194 Taylor diagrams (Taylor, 2001) for the upper 250 m. The normalized standard deviations of
195 modeled variables are shown as the distance from the origin. The correlation between the
196 observations and the modeled parameters is shown by the azimuth angle. The distance between
197 the model points (colors refer to colors in map) and the black observation point (labeled "data")
198 shows the normalized root mean square misfit between the modeled and observed environmental
199 conditions.
200
201 **2.4 Definition of extreme, compound extreme, and triple or quadruple compound extreme**
202 **events**
203 Due to the strong natural variability of the Gulf of Alaska, we chose to use relative
204 thresholds to define the extreme events, assuming that organisms might be adapted to the wide
205 range of variability in their environment. This analysis was based on the daily output of the 28-
206 year-long simulation. First, a 14-day running mean was applied (Figure 5 a and b) to the daily
207 model output (Le Grix et al., 2021), then the seasonal anomalies were computed for each grid
208 cell (Figure 5 c). The relative thresholds were defined as the 95^{th} percentile (Figure 5 d) for
209 temperature and hydrogen ion concentration $[H^+]$ and the 5^{th} percentile aragonite saturation state
210 Ω_{arag} and O_2 of the daily seasonal anomalies as in (Burger et al., 2022). An event was considered
211 as extreme if the anomalies cross the threshold (Figure 5e). A compound extreme event was

defined as the co-occurrence of two (or more) extreme events in time and space (i.e., the same grid cell). Over 10,000 days per grid cell were used to compute percentiles between 1993 and 2021, making the analysis statistically robust. A fixed temporal baseline was used because the strong natural climate variability of the area can mitigate or accelerate the apparent rate of ocean acidification (Hauri et al., 2021), making a moving baseline hard to apply over these relatively short periods of time (less than 30 years). Fixed baselines have been used in several recent studies of extreme events (Barkhordarian et al., 2022; Burger et al., 2022; Desmet et al., 2023; Laufkötter et al., 2020; Le Grix et al., 2021) and are generally well suited to investigate the effect of extreme events on organisms (Oliver et al., 2019). No minimum duration threshold for extreme events was set as it is unknown which thresholds are relevant (Collins et al., 2019; Le Grix et al., 2021).

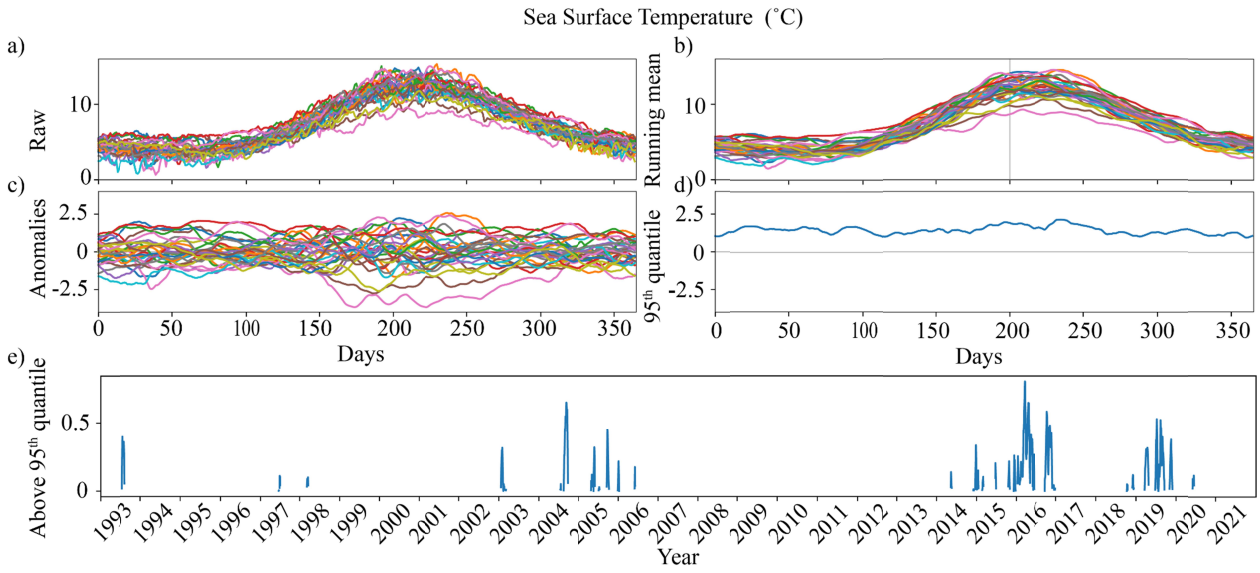

Figure 5. Definition of extreme events. a) Raw daily sea surface temperature data were b) smoothed with a 14-days running mean. c) Seasonal anomalies per grid cell were then used to compute the relative thresholds based on d) the 95th percentile for temperature. e) If an event crosses the relative threshold, it is considered as extreme.

2.5 $[H^+]$ at fixed temperature

$[H^+]$ was computed at a fixed seasonal temperature to highlight the importance of temperature in triggering extreme heat and $[H^+]$ compound extreme events. At each cell grid, $[H^+]$ at a fixed temperature (H^+_{Tfix}) was computed based on the model temperature climatology computed at each cell grid and modeled DIC, TA, and salinity using the PyCO2SYS python package (Humphreys et al., 2022). PyCO2SYS uses the same equations as COBALT to resolve the CO_2 cycle.

2.6 Climate indices

The NGAO index (Figure 1) defined in Hauri et al. (2021) is based on the first mode of variability given by the Empirical Orthogonal Function (EOF) decomposition performed on monthly anomalies (trends and monthly climatology removed) for simulated and satellite observed SSH (Global Ocean Gridded L4 Sea Surface Heights). The Pacific Decadal Oscillation (PDO, Mantua et al., (1997)) index was obtained from https://www.ncei.noaa.gov/pub/data/cmb/ersst/v5/index/ersst.v5.pdo.dat (accessed in May 2023). The North Pacific Gyre Oscillation (NPGO, Di Lorenzo et al., (2008)) index was obtained from http://www.o3d.org/npgo/npgo.php (accessed in May 2023). The Multivariate El Niño/Southern Oscillation (ENSO) index version 2 (MEI.v2) was obtained from https://psl.noaa.gov/enso/mei/data/meiv2.data (accessed in May 2023).

2.7 Extreme event association with various climate indices

To investigate potential relationships of extreme and compound extreme events with different empirical modes of variability (short: "climate modes") we followed the approach of Holbrook et al. (2019) and Le Grix et al. (2021). We computed the frequency of $[H^+]$, Ω_{arag}, and marine heat wave events during the positive, negative, and neutral phases of the PDO, the NPGO, NGAO, and a newly defined downwelling index. The positive phases of each index were associated with days when the indices were above 50 % of their maximum, whereas the negative phases of each index are associated with days the indices were below 50 % of their minimum, and the neutral phases correspond to the days when the indices were between 50 % of their maximum and 50 % of their minimum. To determine if a given climate mode had an effect on extreme event frequencies, we compared the frequency during the positive and negative phases to the frequency during a neutral phase at each grid cell. Finally, to verify the statistical significance we randomly shuffle the temporal order of each index and recomputed the frequency 1,000 times. The result was considered statistically significant if the observed frequency is higher or lower than 95 % of the shuffled cases.

2.8 Definition of the areas used for the extreme and compound extreme events

The areas used in this study were defined based on the spatial pattern of the modeled de-seasonalized sea surface height in the Gulf of Alaska. The seasonal trend was removed from monthly model output and a classical K-MEANS algorithm was applied (Sculley, 2010). The K-MEANS algorithm was configured with four clusters (including the land mask). A silhouette analysis was performed to choose this number of clusters. Prince William Sound, Cook Inlet, and the Juneau areas were discarded since the model has not been specifically designed and evaluated for these near shore areas. The area close to the model lateral boundary (within 50 km)

was also discarded to avoid the direct effect of the boundary conditions on the results. The K-MEANS algorithm defined the following three main areas (Figure 2): (i) the center of the gyre that corresponds to the lowest mean SSH and therefore the maximum upwelling intensity, (ii) the buffer zone between the center of the gyre and the shelf, and (iii) the continental shelf area that corresponds to the area with generally positive SSH (coastal downwelling).

The surface area affected by an event (in %) was computed as a function of each area, every day. The intensity corresponds to the spatial average (over all the grid cells affected by an event) of variable anomalies during an event, every day. The shelf seafloor was defined as the bottom area on the shelf with depths > 50 m and < 250 m.

2.9 Empirical orthogonal function

Empirical orthogonal functions (EOF) were used to determine the modes of variability of the Gulf of Alaska by decomposing the oceanic field into a set of uncorrelated spatial modes (EOFs) and their corresponding temporal variations or principal components (PCs). Following Hauri et al., (2021), the EOF was applied to the sea surface height daily model output after removing the long-term temporal trend and deseasonalizing the data. The results showed that the leading EOF of SSH were well separated based on their eigenvalues with PC1 = 49 % , PC2 = 21 % and PC3 = 12 %.

3 Results and discussion

3.1 Surface heat and acidity compound extreme events in the Gulf of Alaska

The Gulf of Alaska ecosystem experienced the first heat and positive [H^+] compound extreme events during the 2013-2016 marine heat wave (Figures 6a and 7a). While several marine heat waves occurred throughout the simulation, the 2013-2016 and 2018-2020 marine

heat waves lasted longer and were more extreme than the previous ones, which aligns with previous observational and modeling studies (Amaya et al., 2020; Di Lorenzo & Mantua, 2016). The 2013-2016 marine heat wave was preceded by a 7-year-long cold phase (Danielson et al., 2022), with frequent low Ω_{arag} and high [H^+] extreme events that affected a large proportion of the gyre area (Figure 6a-c and d-f; Hauri et al., (2021). Negative Ω_{arag} extreme events also affected up to 95 % of the surface water on the shelf at times (Figure 6c), whereas positive [H^+] extreme events were not as pronounced there (Figure 6b). This rapid succession of positive [H^+], negative Ω_{arag}, and heat extreme events that started in the early 2000s was followed by several marine heat and positive [H^+] compound extreme events, constantly exposing the ecosystem to environmental conditions outside their norm. During the 2013-2016 marine heat wave, the gyre area experienced on average 19 (+/- 15, STD) days of these compound extreme events and up to 88 days for some grid cells. The marine heat and positive [H^+] compound extreme events lasted longer on the shelf, with a mean of 55 (+/- 32) days and a maximum of 146 days. During the peak of the marine heat wave, when the intensity was highest and the entire shelf area was affected by extreme heat, 60 % of the shelf area experienced a marine heat and positive [H^+] compound extreme event. The 2018-2020 marine heatwave already started in late 2018 (Figures 6a and 7a) and therefore earlier in the Gulf of Alaska than in other parts of the North Pacific, which corresponds with observations by Amaya et al., (2020). The number of days affected by marine heat and positive [H^+] compound extreme events over the gyre area increased twofold during the 2018-2020 marine heatwave compared to the 2013-2016 marine heat wave. Up to 50 % of the gyre region was affected by those extreme conditions that lasted on average 41 (+/- 32) days and up to 41 % of the shelf ecosystem was exposed over an average of 59 (+/- 39) days. In

319 contrast, short extreme heat and negative Ω_{arag} compound extreme events only occurred during
320 the 2019-2020 marine heat wave and affected small portions of the shelf (<10 %, Figure 6e).
321
322
323
324

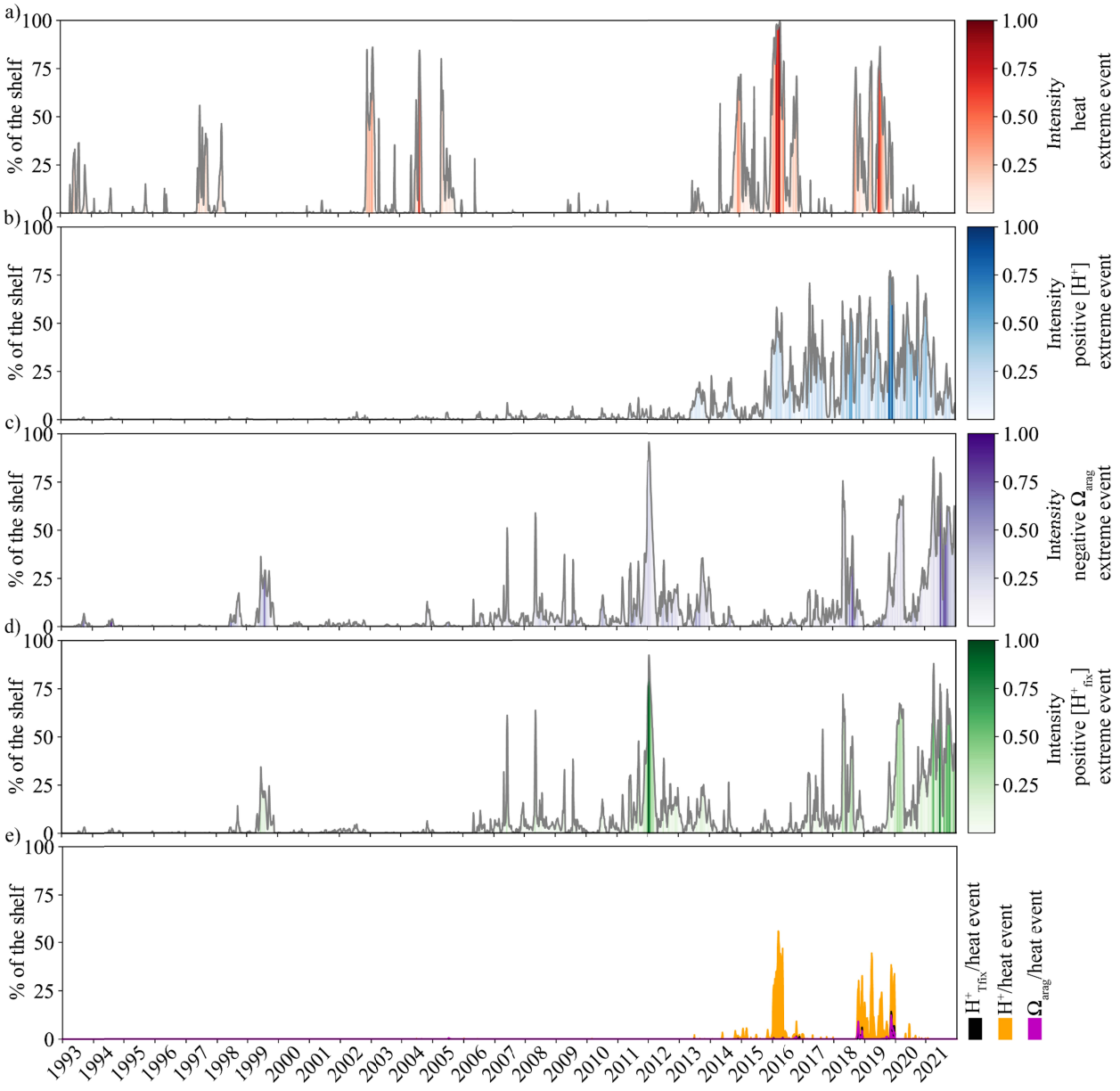

325

Figure 6. Timing of sea surface marine heat and acidity extreme and compound extreme events over the shelf area. Area affected by (%) of a) marine heat (red), b) positive [H^+] (blue), c) negative Ω_{arag} (purple), d) positive [H^+] at fixed seasonal temperature (Tfix, green) extreme events, and e) positive [H^+] and marine heat (orange), positive [H^+] at fixed temperature and marine heat (black), negative Ω_{arag} and marine heat (purple) compound extreme events. The color bars indicate the intensities of the events.

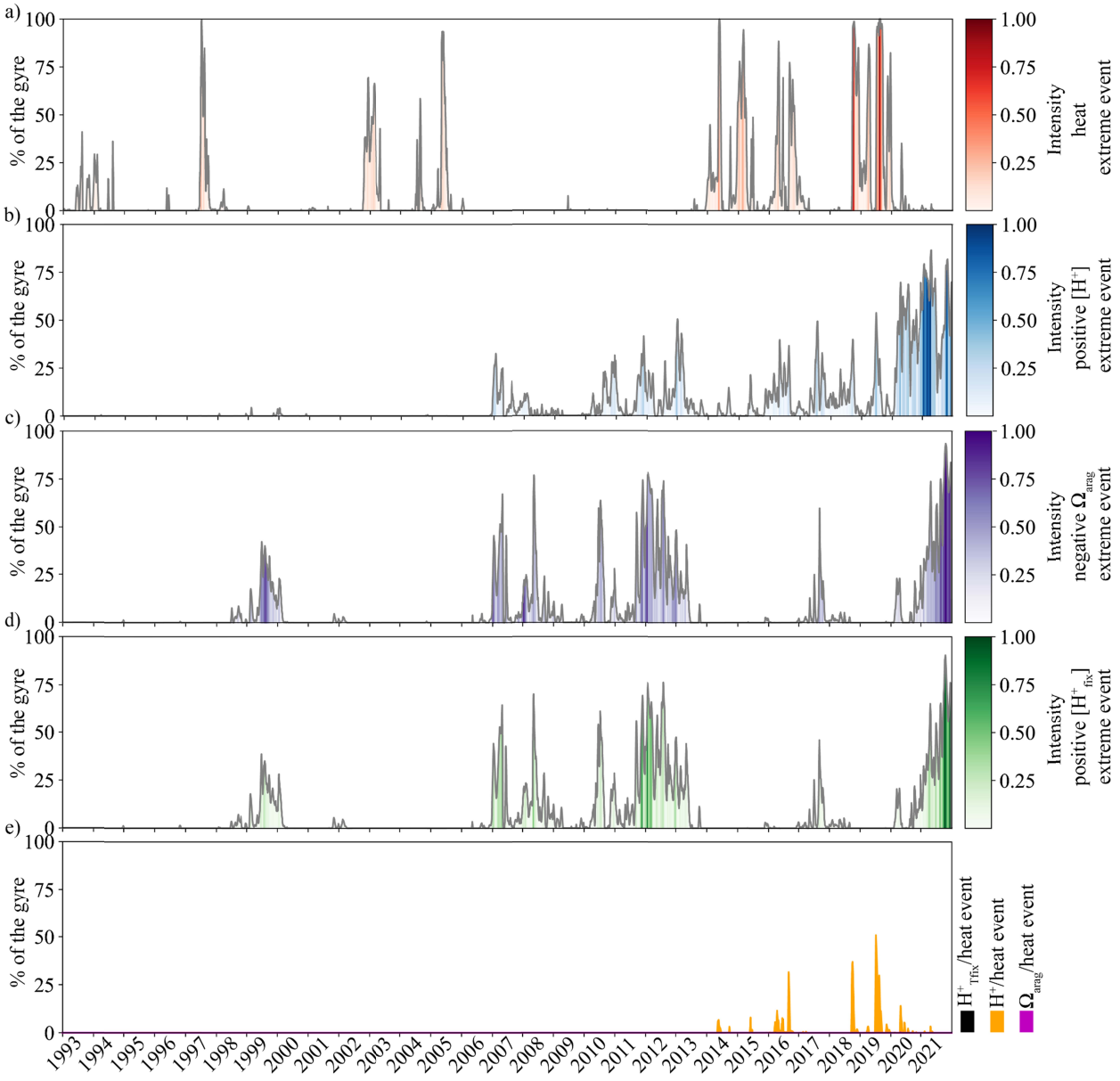

Figure 7. Timing of sea surface marine heat and acidity extreme and compound extreme

events over the gyre area. Area affected by (%) of a) marine heat (red), b) positive [H^+] (blue), c) negative Ω_{arag} (purple), d) positive [H^+] at fixed temperature (Tfix, green) extreme events, and e) positive [H^+] and marine heat (orange), positive [H^+] at fixed temperature and marine heat (black), negative Ω_{arag} and marine heat (purple) compound extreme events. The color bars indicate the intensities of the events.

3.2 Temperature induced early onset of heat and positive [H^+] compound extreme events

While [H^+] and Ω_{arag} both follow a secular trend as a result of ocean acidification, the intensity and extent of positive [H^+] and negative Ω_{arag} extreme events were spatially and temporally decoupled as a result of their sensitivity to different climate change and natural variability-affected physical drivers (Figures 6, 7 and 8). The natural climate variability of the offshore upwelling, described by the local climate index NGAO, directly affects extreme and compound extreme events at the surface (Figure 8). For example, during negative NGAO events (2006-2012, Figure 1) strong offshore upwelling of cold, CO_2-rich subsurface water in the Alaska gyre leads to both positive [H^+] and negative Ω_{arag} extreme events, although negative Ω_{arag} extreme events were more intense and covered a wider area in the gyre (Figure 6 b and h ; Hauri et al., 2021). Negative Ω_{arag} extreme events also occurred on the shelf (Figure 6 c), whereas positive [H^+] extreme events were less common there (Figure 6b). It is important to understand the underlying cause of extreme acidity events. Because of the complexity of seawater acid-base chemistry, elevated acidity can occur either because of more CO_2-rich water or because of warmer temperature with fixed inorganic carbon and alkalinity. At fixed seasonal temperature (Figures 6 and 7d), positive [H^+] extreme events increased in the gyre (Figure 7d)

357 and expanded onto the shelf (Figure 6 d), following a similar pattern as the positive Ω_{arag} extreme
358 events. This suggests that during a negative NGAO phase, offshore upwelling of cold subsurface
359 water (Figure 9) dampened the signal of $[H^+]$-rich upwelled water and thus the strength and
360 extent of positive $[H^+]$ extreme events in the gyre and on the shelf.

361 Elevated temperature during the positive NGAO phase amplified elevated $[H^+]$
362 concentrations to trigger the first surface marine heat and positive $[H^+]$ compound extreme
363 events in the shelf region. During a positive NGAO phase (e.g., marine heat waves in 2013 -
364 2016 and 2018-2020, Figure 1) upwelling was less intense, which led to warmer (Figure 9) and
365 less acidic conditions in the gyre. This natural mechanism preconditioned the water and caused
366 the early onset of the 2018-2020 marine heat wave in the Gulf of Alaska. Simultaneously, it
367 weakened positive $[H^+]$ and negative Ω_{arag} extreme events in the gyre region during the positive
368 NGAO phase (Figure 8d). However, elevated temperature in the positive NGAO phases
369 increased $[H^+]$ concentrations enough to cause $[H^+]$ extreme events on the shelf, triggering the
370 first marine heat and positive $[H^+]$ compound extreme events. At fixed temperature, positive $[H^+]$
371 extreme events did not occur on the shelf during positive NGAO phases (Figure 8h). In the gyre,
372 the generally colder conditions (Figure 3a,b) resulting from persistent upwelling activity
373 tampered $[H^+]$ events, even during NGAO positive phases.

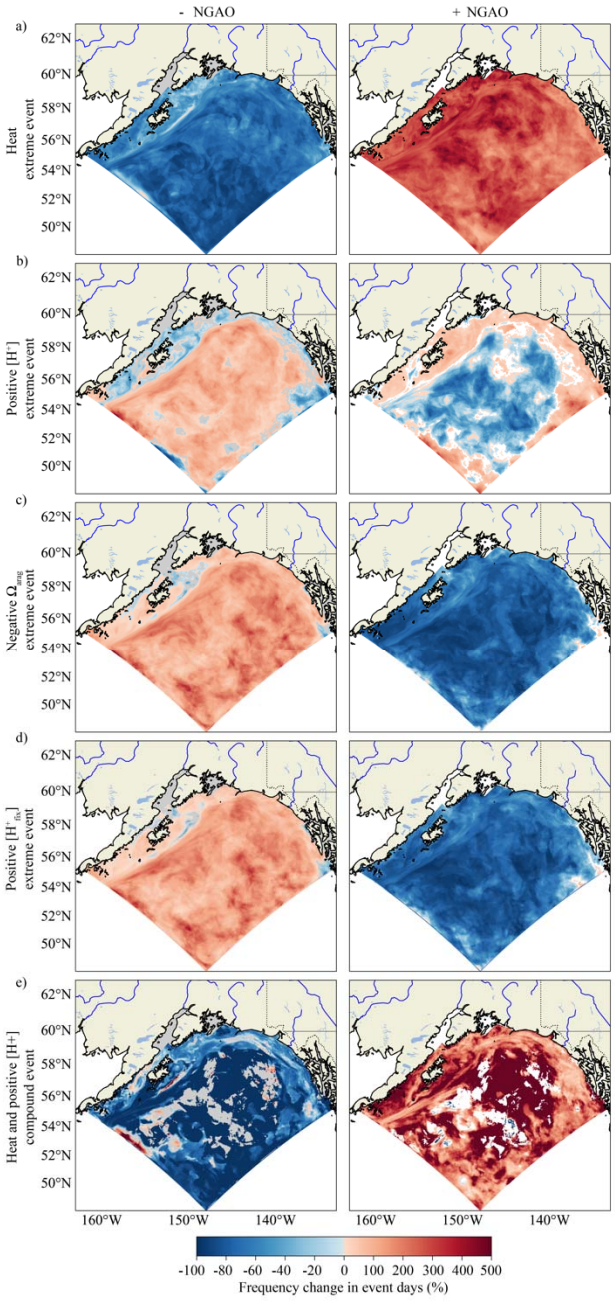

374

375 **Figure 8. The role of internal climate variability in the occurrence of extreme and**

376 **compound extreme marine heat and acidity events.** Frequency change in event days during

377 negative (left) and positive (right) phases of the Northern Gulf of Alaska Oscillation (NGAO,

378 Hauri et al. (2021)) compared to their frequency during a neutral phase for marine heat (a),

379 positive [H^+] (b), negative Ω_{arag} (b), positive [H^+] with fixed temperature (d) extreme events, and

for heat and positive [H^+] compound extreme events (e). White cells are not statistically significant (significance level set as 95%).

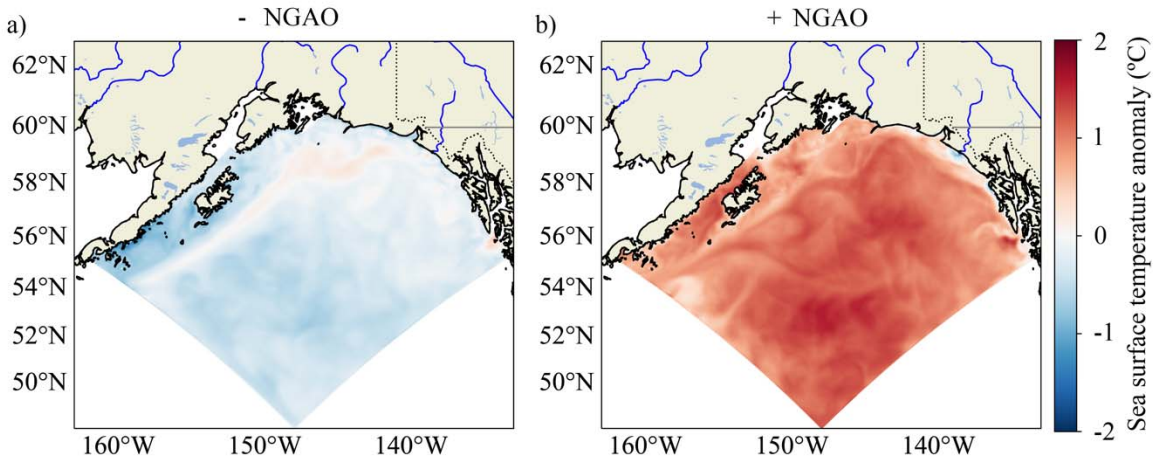

Figure 9. Impact of the Northern Gulf of Alaska Oscillation on summertime temperature. Sea surface temperature (℃) anomaly in summer (June - August) during positive (left) and negative (right) Northern Gulf of Alaska (NGAO) phases between 1993 and 2021. The positive and negative phases of the NGAO index are associated with days when the index was above 50 % of its maximum or below 50 % of its minimum.

3.3 Triple and quadruple compound extreme events on shelf seafloor

The environment on the shelf seafloor also experienced extremely high [H^+], and extremely low Ω_{arag}, and O_2 conditions during the 2013-2016, and more intensely during the 2018-2020 marine heat wave, causing quadruple compound extreme events. Marine heat extreme events occurred throughout the timeseries, but became more prevalent during the 2013-2016 marine heat wave and affected up to 80 % of the seafloor (Figure 10a). This subsurface marine heat wave started in 2015 and therefore later than at the surface, which is consistent with *in situ* observations (Danielson et al., 2022). The timing of our modeled heat waves on the shelf

seafloor is also similar to the timing of events found in an ocean reanalysis study (Amaya et al., 2023), although they used the 90th percentile and considered a larger shelf area (bottom grid cells shallower than 400 m), which could have led to the differences in the spatial extent and duration of the heat waves. Triple positive [H^+], negative Ω_{arag}, and negative O_2 compound extreme events covered > 20 % of the area in 2005 and increased in frequency, intensity, and spatial extent over time (Figure 10 f), and especially during the 2013-2016 and 2018-2020 marine heat waves. Those triple events affected up to 38 % and 47 % of the seafloor area over an average of 108 (+-65) and 135 (+-68) days respectively between 2013-2016 and 2018-2020. Positive [H^+], negative Ω_{arag}, and negative O_2 compound extreme events co-occurred with extreme heat events sporadically for the first time during the 2013-2016 marine heat wave (1 % of the benthic area affected), and frequently during the 2018-2020 marine heat wave, thereby forming quadruple compound extreme events (Figure 10f). Quadruple extreme events covered up to 26 % of the shelf seafloor area over an average of 40 (+-32) days.

3.4 Quadruple extreme events on shelf seafloor were driven by anthropogenically amplified CO_2 concentrations in deep water intrusion

The interaction between marine heat waves (remotely triggered) and the local natural variability of deep-water intrusion triggered positive [H^+] and heat, negative Ω_{arag}, and negative O_2 quadruple compound extreme events on the shelf seafloor. Intrusion of deep, salty, CO_2-rich, and O_2-poor water can be approximated through the intensity of coastal downwelling and therefore is indicated by sea surface height variations. The second mode of variability of sea surface height in our model domain, here defined as the Gulf of Alaska downwelling index (GOADI), can be used as a proxy for the coastal downwelling strength. A positive phase indicates increased sea

surface height and therefore strong downwelling and weak or no intrusion of deep and colder water onto the shelf. A negative phase shows relaxation of downwelling and intrusion of deeper and colder water onto the shelf. Higher salinities on the shelf have been linked to relaxation of downwelling and deep-water intrusion onto the shelf (Danielson et al., 2022; Ladd et al., 2005; Stabeno et al., 2016). Modeled positive salinity events are highly correlated with positive [H^+] with a Pearson correlation coefficient (Pcc) of 0.65 (p-value <0.01), and with negative Ω_{arag} (Pcc = 0.63, p-value <0.01) and O_2 (Pcc = 0.8 p-value <0.01) and exhibit the same temporal variability even though their intensity and affected area can slightly differ. During a negative phase (weak downwelling activity) the frequency of positive [H^+] and negative Ω_{arag}/O_2 triple compound extreme events strongly increases (Figure 12 b-f). In contrast, the heat extreme events are dampened during this phase (Figure 12a). For example, the intense 2016 marine heatwave along the shelf seafloor is weakened as the downwelling relaxes toward the end of the year (downwelling index flips from strongly positive to negative), which suggest that intrusion of cold water alleviated this sub-surface marine heat wave. During a positive phase (strong downwelling activity), positive [H^+], and negative Ω_{arag}/O_2 triple compound extreme events are suppressed while the intensity and occurrence of marine heatwaves on the shelf seafloor tends to increase. Assuming GOADI can be represented by a first-order autoregressive [AR(1)] process , we observe a relatively short memory of the index with an inverse damping rate λ^{-1} of ~1.7 months (calculated via the 1-month lag autocorrelation *r*, with $\lambda = -\ln(r)/\Delta t$).

Quadruple events on the shelf seafloor are induced by a combination of remotely triggered heatwaves, secular ocean acidification trend and locally controlled relaxation of downwelling. Triple positive [H^+], and negative Ω_{arag}/O_2 compound extreme events occurred for the first time in a widespread manner in 2004/2005 (> 20 % of shelf area) and increased in

443 frequency, intensity, and spatial extent over time (Figure 10f), and especially during the two
444 most recent heat waves. These triple events are mainly triggered due to the secular trend of ocean
445 acidification, as there were less positive [H^+] (area increased by 1 % per year) and negative Ω_{arag}
446 (0.85 %/year) extreme events at the beginning of the timeseries. It is not likely that the intensity
447 and frequency of deep-water intrusion has changed over the years, although the current
448 timeseries may be too short to detect secular trends (Hauri et al., 2021). While both marine heat
449 waves (2015-2016 and 2019-2020) affected > 80% of the seafloor on the continental shelf,
450 widespread (>20 % of shelf area) quadruple events with compound marine heat, positive [H^+],
451 and negative Ω_{arag}/O_2 quadruple extremes only occurred during the second marine heat wave in
452 2019. During this time, the downwelling index was generally negative, and triggered intrusion of
453 deeper, colder, CO_2 rich, and O_2 poor water onto the shelf. While the colder water dampened the
454 intensity of the benthic heat wave, it was not enough to avoid the occurrence of quadruple
455 compound extreme events across > 20 % of the shelf area.
456
457 **3.5 What does this mean for the Gulf of Alaska marine ecosystem?**
458 The Gulf of Alaska marine community experienced dramatic shifts during 2014-2016 and
459 2019 period, with continued and/or lagged impacts still present in the ecosystem (Suryan et al.,
460 2021). The impact on commercially valuable groundfish varied by species. Gulf of Alaska
461 Pacific cod (*Gadus microcephalus Tilesius*) experienced a 71% decline in abundance in 2017
462 and a commercial fishery closure in 2020 (Barbeaux et al., 2020). Conversely, Alaska sablefish
463 (*Anoplopoma fimbria*) had strong year classes from 2014 to 2019, and 2016 was potentially the
464 largest recruitment recorded (Goethel et al. 2022). Other changes throughout the ecosystem
465 included reduced primary production, changes in zooplankton community composition, reduced

466 forage fish abundance during the 2014-2016 period followed by a strong and persistent herring
467 year class in 2016 (Arimitsu et al., 2021; Strom 2023), and increased mortality and reduced
468 reproductive success of seabirds and marine mammals (Hastings et al., 2023; Piatt et al., 2020).
469 The ecological changes during and after this period have primarily been attributed to
470 prolonged, elevated ocean temperatures, yet the consideration of dissolved oxygen and pH may
471 also explain ecosystem changes not yet identified or understood. The warm ocean temperatures
472 are suggested to have affected Pacific cod by exceeding optimal thermal thresholds of cod egg
473 and larval survival (Laurel et al., 2023), and increased metabolic rates, resulting in increased
474 oxygen demand and consumption rates in a reduced prey environment (Barbeaux et al., 2020).
475 However, the cod population has not yet rebounded, despite the return of pre-marine heatwave
476 ocean temperatures and prey abundance, suggesting missing pieces to the narrative. During this
477 time period, some groundfish species shifted to deeper (and therefore cooler) habitats, while
478 others moved to shallower depths (presumably warmer), suggesting the presence of other
479 environmental drivers and restrictions (Yang et al., 2019). Rockfish living deeper along the GOA
480 slope, such as adult thornyhead rockfish (*Sebastolobus spp.*; 100-1,200 m), rougheye (*S.*
481 *aleutianus*) and blackspotted (*S. melanostictus*) rockfish (300-500 m), and shortraker rockfish (*S.*
482 *borealis*; 300-400 m), live in lower oxygen environments and are predicted to potentially move
483 shallower (perhaps into warmer temperatures) if oxygen concentrations decrease further
484 (Thompson et al., 2023). Lower pH could result in a decline of biomass or condition of deep-
485 water corals, important habitat for juvenile Pacific Ocean perch (*S. alutus*) and numerous other
486 commercially important rockfish. Increased acidity can also be detrimental to pteropods, a
487 calcifying organism and common prey for pink salmon. Pink salmon are predicted to decline in
488 growth and population size if a reduction in pteropod biomass occurs (Aydin et al., 2005).

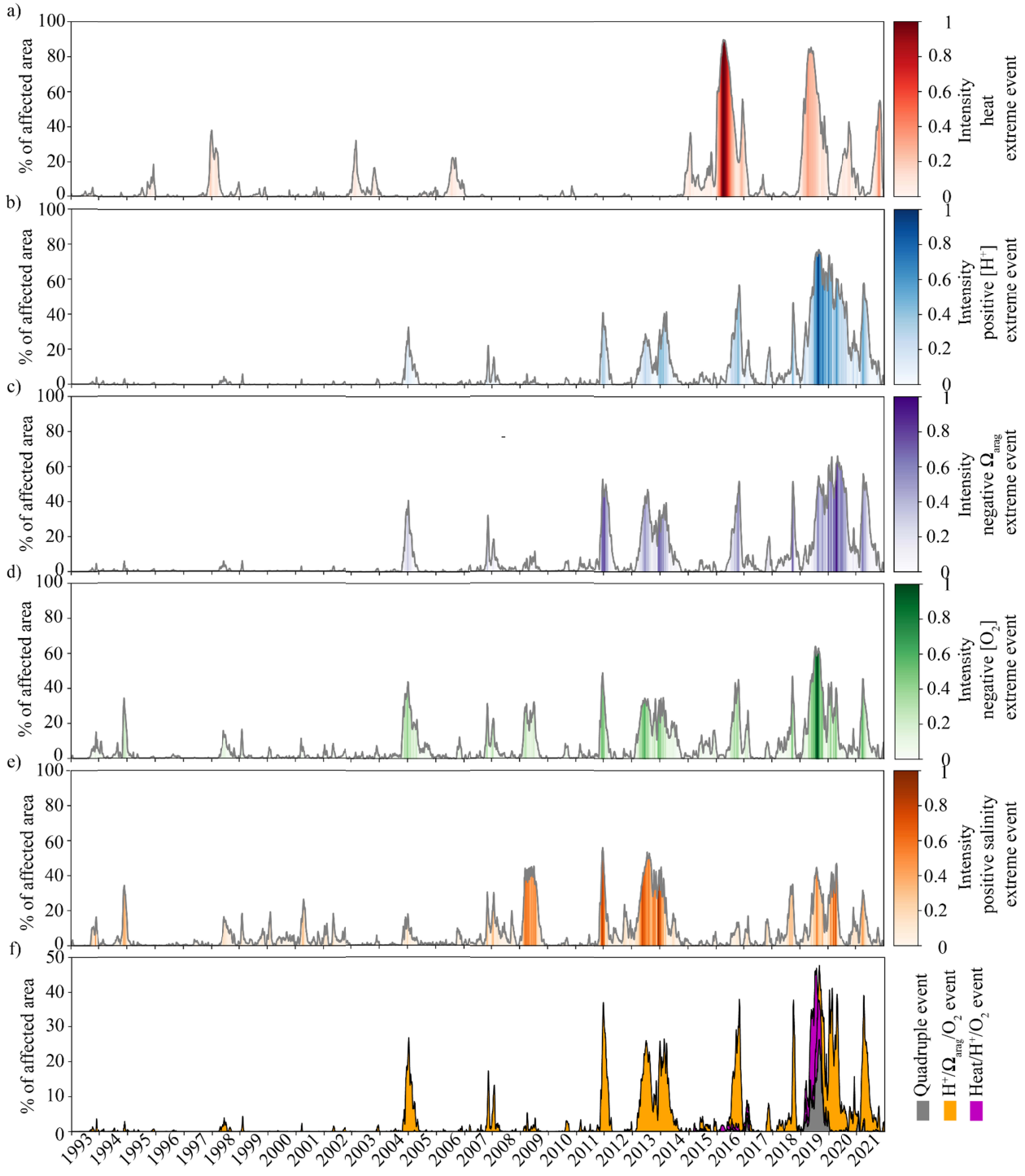

Figure 10. Timing of marine heat, acidification, and low oxygen extreme and compound extreme events at the shelf seafloor. Area (%) affected by a) marine heat (red), b) positive [H^+]

493 (blue), c) [H^+], negative Ω_{arag} (blue), d) negative oxygen (green), and e) triple (orange: negative
494 oxygen, positive [H^+], negative Ω_{arag}, purple: negative oxygen, positive [H^+], heat), and
495 quadruple compound extreme events (negative oxygen, positive [H^+], heat, negative Ω_{arag}). The
496 color bars indicate the intensities of the marine heat, acidification, and low oxygen extreme
497 events in red, blue, purple, and green, respectively. The benthic area on the shelf is defined as the
498 area with a bottom depth between 50 m to 250 m depth.
499

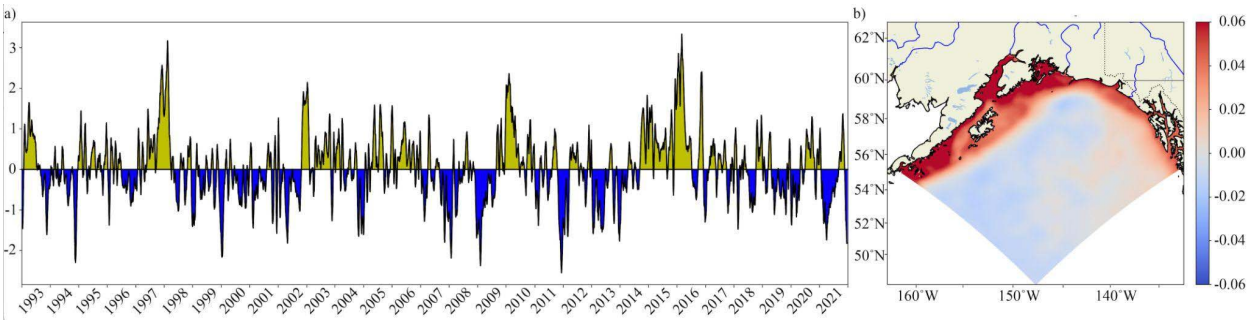

500
501

502 **Figure 11. Gulf of Alaska Downwelling Index (GOADI) as indicator for environmental**
503 **conditions on shelf seafloor.** Time series (a) of the normalized principal component associated
504 with the second Empirical Orthogonal Function (EOF) mode of sea surface height. Maps of the
505 EOF (b) spatial patterns of the second mode of sea surface height (SSH, m). The amount of
506 variance associated with the second EOF is ~ 9.5 %. The EOFs were computed based on the
507 illustrated spatial domain and were applied to daily model output after first removing a long-term
508 temporal trend using a quadratic function and second deseasonalizing the data.
509

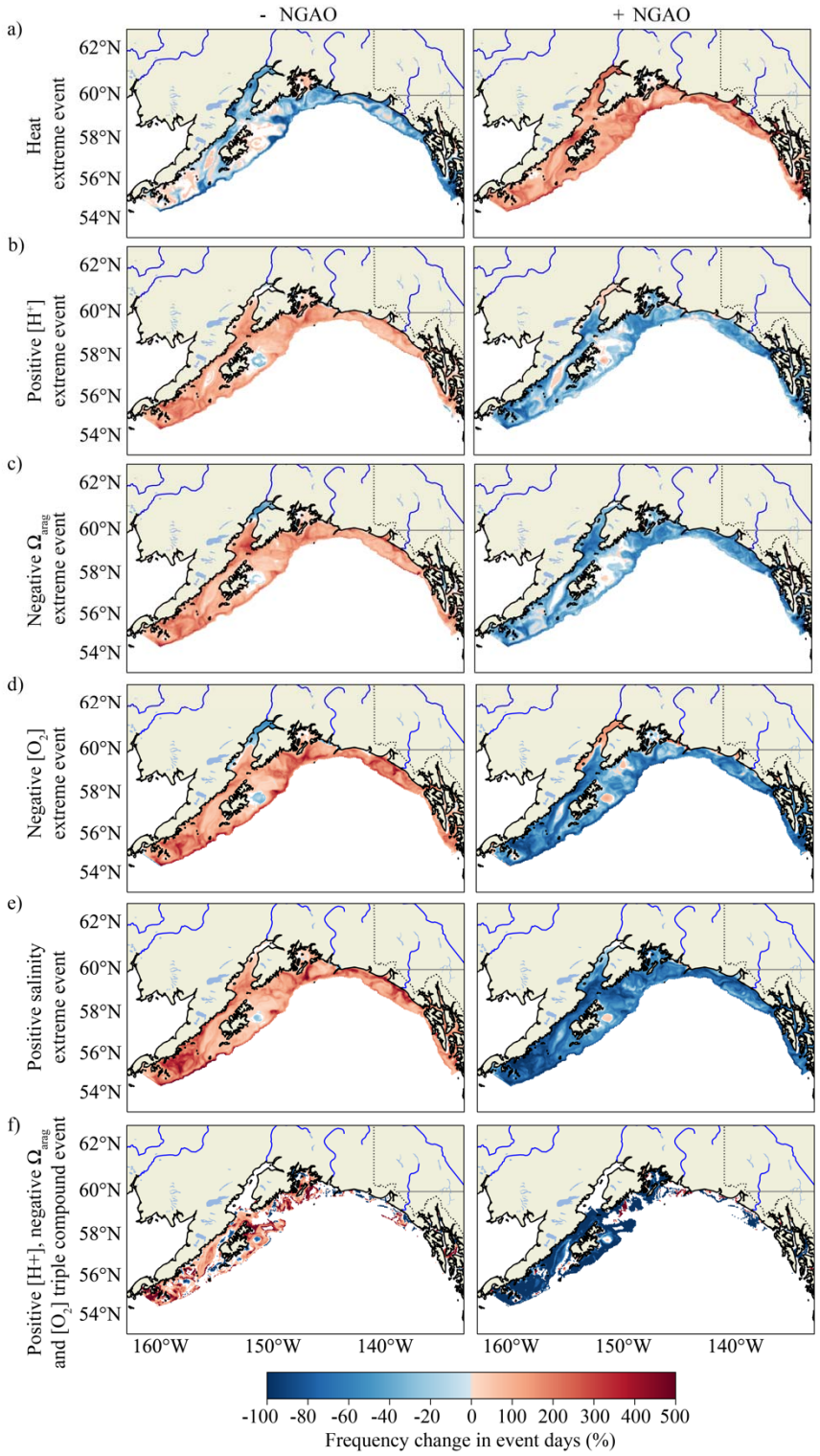

510

511 **Figure 12. The role of internal climate variability in the occurrence of extreme and**

512 **compound extreme events on shelf seafloor.** Frequency change in event days during negative

(left) and positive (right) phases of the Northern Gulf of Alaska Oscillation (NGAO, Hauri et al., (2021)) compared to their frequency during a neutral phase for a) marine heat extreme events, b) positive [H^+] extreme events, c) negative Ω_{arag} extreme events, d) negative [O_2] extreme events, e) positive salinity extreme events, and f) positive [H^+], and negative Ω_{arag}/O_2 triple compound extreme events. White cells are not statistically significant (significance level set as 95%).

3.5 Usefulness of our statistical approach

The metrics applied here and in previous extreme event studies (Barkhordarian et al., 2022; Gruber et al., 2021; Laufkötter et al., 2020; Le Grix et al., 2021) should be seen as a "probability of trouble" rather than a true indicator of stress. Stress can be defined as a condition evoked in an organism by one or more environmental factors that brings the organism near or over the limit of its ecological niche (Van Straalen, 2003). The biological consequence of a particular stress response depends on its intensity and duration (Boyd et al., 2018). A threshold is the limit beyond which stress and detrimental effects are expected for any environmental parameters such as temperature, carbonate chemistry, or oxygen concentration (IOC-UNESCO, 2022). However, based on our understanding of the biological response to environmental changes, no simple or absolute thresholds are expected. First, these will vary depending on locations (e.g., local adaptation; Vargas et al. (2017, 2022)). A threshold for a given parameter will also be modulated by other environmental conditions. For example, the pH threshold for sea urchin larvae is strongly influenced by temperature and a higher pH threshold is observed at low temperature (Gianguzza et al., 2014). Complex threshold landscapes emerge because no common thresholds exist, and due to local adaptation and combined effects between environmental parameters (Boyd et al., 2018). Relative thresholds allow to account for adaptation to the local range of natural variability of a given variable and assume that the organism is jeopardized by

variation outside of this natural range. Relative thresholds have been frequently used to define marine heat waves (Barkhordarian et al., 2022; Gruber et al., 2021; Laufkötter et al., 2020; Le Grix et al., 2021) as well as ocean acidity extreme events (Burger et al., 2020; Desmet et al., 2023; Gruber et al., 2021). While relatively easy to calculate and based on a good theoretical framework, this approach does not fully integrate the complexities driving local species and ecosystem sensitivities, and often ignores the physiological, ecological and evolutionary consequences of subsequent or compound extreme events (Gruber et al., 2021). As a consequence, we are still lacking the level of understanding to be sure that the extreme and compound extreme events computed here and in previous studies are leading to a true stress. In other words, we cannot assume that the calculated "index" can correlate to a measure of stress. Nevertheless, mapping the spatial and temporal occurrence of environmental extremes and understanding their drivers is an important exercise. First, based on what we know, it is likely that extreme events are leading to stress and when it comes to stressors, two stressors are always worse than one (by definition). So, while we cannot infer the biological response, the probability of negative effects on marine life is there. Second, knowing where, when, and why compound extreme events occur should inform mitigation strategies and improve the predictability of such events.

Translating extremes in environmental conditions to a biological response would require more than a correlation between physical-chemical and biological observations. It can only be achieved through a coordinated combination of monitoring, field and laboratory experimentation, and modeling. It would require a strong dialogue between different disciplines such as modeling, physical, biogeochemical and biological observations, experimental biology, physiology, ecology, and multiple stressors. For example, laboratory experiments should focus on

mechanistic understanding of the impact of each key drivers to resolve their mode of action and performance curves under extreme conditions (e.g., heat, positive [H^+], negative O_2, and negative Ω_{arag} stress), the role of intensity/duration, and the relative contribution of each parameter on the response. For example, temperature, pH and oxygen are impacting the physiology and metabolism of marine organism and can lead to mortality under extreme conditions. However, it is unclear what the characteristic of a marine heat extreme events are that would drive similar response than a given acidity extreme event. Such a mechanistic understanding at different levels of organization would allow one to understand and model their combined effects. This could lead to a "formula" that would translate the physical-chemical characteristics of the extreme and compound extreme events into a "stress index" and the biological consequences. Combining this mechanistic understanding with modeling could ultimately explain the observed ecological changes (IOC-UNESCO, 2022) and project future changes.

4 Summary and Conclusions

The Gulf of Alaska has been exposed to several marine heat waves, which were associated with devastating consequences for the marine ecosystem. Our modeling results suggest that during these marine heat waves ocean acidity and oxygen levels also reached levels outside of the natural variability envelope and thereby may have played a role in the observed ecosystem effects.

A mechanistic understanding of compound extreme events and their consequences is necessary to implement local mitigation and adaptation strategies. Our results show that local climate variability in combination with remote teleconnections and secular trends of ocean acidification and warming led to the manifestation of these compound extreme events. We are now able to use the readily available indices NGAO and GOADI to better describe past and

584 future environmental conditions, which provides the opportunity to directly study what effects
585 these combined extreme environmental conditions may have on the ecosystem.
586 Prediction and projection of environmental conditions and ecosystem change are a
587 necessary next step to support adaptation and fisheries management decisions in the Gulf of
588 Alaska marine ecosystem. Seasonal forecasts would support quota management on an annual
589 basis, whereas regional long-term projections would provide insights into how local and remote
590 drivers of extreme events will manifest themselves under a changing climate.
591

592 **Acknowledgement**

593 Our study covers the Gulf of Alaska marine environment, which is in the traditional and
594 contemporary unceded homelands of the Haida, Tsimshian, Tlingit, Eyak, Dena'ina,
595 Sugpiaq/Alutiiq, and Unangax̂/Aleut Peoples. Moreover, the offices of the University of Alaska
596 Fairbanks are located on the unceded Native lands of the Lower Tanana Dena. We are grateful to
597 the Indigenous communities, who have been in deep connection with their land and water for
598 now and time immemorial, for the stewardship of their environment. We also recognize the
599 historical and ongoing legacies of colonialism and are committed to improve equity in our lives
600 and scientific institutions we work with. The authors acknowledge support from the North
601 Pacific Research Board (NPRB 2109) and National Science Foundation (OIA-1757348, OCE-
602 1656070). This study has been conducted using E.U. Copernicus Marine Service Information;
603 https://doi.org/10.48670/moi-00021, https://doi.org/10.48670/moi-00016,
604 https://doi.org/10.48670/moi-00148.
605

606 **Data availability**

The model output is publicly available (DOI here).

Code availability

The ROMS-COBALT source codes used in this study are available at: 10.5281/zenodo.3647609 (Hedstrom et al., 2020). Configuration files are available at 10.5281/zenodo.8316392 (Pages et al., 2023). The scripts used to compute the extreme events and define the areas are available at 10.5281/zenodo.8291232 (Pages, 2023) and the scripts used to attribute extreme events to climate modes are available at 10.5281/zenodo.4542015 (Le Grix, 2021).

Conflict of Interest

The authors declare no conflicts of interest relevant to this study.

References

Amaya, D. J., Miller, A. J., Xie, S.-P., & Kosaka, Y. (2020). Physical drivers of the summer 2019 North Pacific marine heatwave. *Nature Communications*, *11*(1), 1903. https://doi.org/10.1038/s41467-020-15820-w

Amaya, D. J., Jacox, M. G., Alexander, M. A., Scott, J. D., Deser, C., Capotondi, A., & Phillips, A. S. (2023). Bottom marine heatwaves along the continental shelves of North America. *Nature Communications*, *14*(1), 1038. https://doi.org/10.1038/s41467-023-36567-0

Arimitsu, M. L., Piatt, J. F., Hatch, S., Suryan, R. M., Batten, S., Bishop, M. A., et al. (2021). Heatwave-induced synchrony within forage fish portfolio disrupts energy flow to top pelagic predators. *Global Change Biology*, *27*(9), 1859–1878. https://doi.org/10.1111/gcb.15556

630 Aydin, K. Y., McFarlane, G. A., King, J. R., Megrey, B. A., & Myers, K. W. (2005). Linking
631 oceanic food webs to coastal production and growth rates of Pacific salmon
632 (Oncorhynchus spp.), using models on three scales. *Deep Sea Research Part II: Topical*
633 *Studies in Oceanography*, *52*(5–6), 757–780. https://doi.org/10.1016/j.dsr2.2004.12.017
634 Barbeaux, S. J., Holsman, K., & Zador, S. (2020). Marine heatwave stress test of ecosystem-
635 based fisheries management in the Gulf of Alaska Pacific cod fishery. *Frontiers in*
636 *Marine Science*, *7*. https://www.frontiersin.org/articles/10.3389/fmars.2020.00703
637 Barkhordarian, A., Nielsen, D. M., & Baehr, J. (2022). Recent marine heatwaves in the North
638 Pacific warming pool can be attributed to rising atmospheric levels of greenhouse gases.
639 *Communications Earth & Environment*, *3*(1), 1–12. https://doi.org/10.1038/s43247-022-
640 00461-2
641 Beamer, J. P., Hill, D. F., Arendt, A., & Liston, G. E. (2016). High-resolution modeling of
642 coastal freshwater discharge and glacier mass balance in the Gulf of Alaska watershed.
643 *Water Resources Research*, *52*(5), 3888–3909. https://doi.org/10.1002/2015WR018457
644 Bednaršek, N., Naish, K.-A., Feely, R. A., Hauri, C., Kimoto, K., Hermann, A. J., et al. (2021).
645 Integrated Assessment of Ocean Acidification Risks to Pteropods in the Northern High
646 Latitudes: Regional Comparison of Exposure, Sensitivity and Adaptive Capacity.
647 *Frontiers in Marine Science*, *8*. https://doi.org/10.3389/fmars.2021.671497
648 Bell, D. A., Kovach, R. P., Robinson, Z. L., Whiteley, A. R., & Reed, T. E. (2021). The
649 ecological causes and consequences of hard and soft selection. *Ecology Letters*, *24*(7),
650 1505–1521. https://doi.org/10.1111/ele.13754

651 Bellquist, L., Saccomanno, V., Semmens, B. X., Gleason, M., & Wilson, J. (2021). The rise in
652 climate change-induced federal fishery disasters in the United States. *PeerJ*, *9*, e11186.
653 https://doi.org/10.7717/peerj.11186
654 Bond, N. A., Cronin, M. F., Freeland, H., & Mantua, N. (2015). Causes and impacts of the 2014
655 warm anomaly in the NE Pacific. *Geophysical Research Letters*, *42*(9), 3414–3420.
656 https://doi.org/10.1002/2015GL063306
657 Boyd, P. W., Collins, S., Dupont, S., Fabricius, K., Gattuso, J. P., Havenhand, J., et al. (2018).
658 Experimental strategies to assess the biological ramifications of multiple drivers of global
659 ocean change - a review. *Global Change Biology*, *24*, 2239–2261.
660 https://doi.org/10.1111/gcb.14102
661 Boyer, Tim P.; Garcia, Hernan E.; Locarnini, Ricardo A.; Zweng, Melissa M.; Mishonov, Alexey
662 V.; Reagan, James R.; Weathers, Katharine A.; Baranova, Olga K.; Seidov, Dan;
663 Smolyar, Igor V. (2018). World Ocean Atlas 2018. NOAA National Centers for
664 Environmental Information. Dataset. https://www.ncei.noaa.gov/archive/accession/NCEI-
665 WOA18. Accessed [08-08-2023].
666 Breitberg, D., Salisbury, J., Bernhard, J., Cai, W.-J., Dupont, S., Doney, S., et al. (2015). And on
667 top of all that… Coping with ocean acidification in the midst of many stressors.
668 *Oceanography*, *25*(2), 48–61. https://doi.org/10.5670/oceanog.2015.31
669 Burger, F. A., John, J. G., & Frölicher, T. L. (2020). Increase in ocean acidity variability and
670 extremes under increasing atmospheric CO_2; *Biogeosciences*, 17, 4633–4662.
671 https://doi.org/10.5194/bg-17-4633-2020

672 Burger, F. A., Terhaar, J., & Frölicher, T. L. (2022). Compound marine heatwaves and ocean
673 acidity extremes. *Nature Communications*, *13*(1), 4722. https://doi.org/10.1038/s41467-
674 022-32120-7
675 Collins, M., M. Sutherland, L. Bouwer, S.-M. Cheong, T. Frölicher, H. Jacot Des Combes, M.
676 Koll Roxy, I. Losada, K. McInnes, B. Ratter, E. Rivera-Arriaga, R.D. Susanto, D.
677 Swingedouw, and L. Tibig. (2019). *Extremes, Abrupt Changes and Managing Risk, in:*
678 *IPCC Special Report on the Ocean and Cryosphere in a Changing Climate* (1st ed.).
679 Cambridge University Press. https://doi.org/10.1017/9781009157964
680 Cooley S, Schoeman D, Bopp L, Boyd P, Donner S, Ito S, et al., (2022) Oceans and Coastal
681 Ecosystems and their Services. In IPCC AR6 WGII. Cambridge University Press. pp.
682 379-550.
683 Coyle, K. O., Hermann, A. J., & Hopcroft, R. R. (2019). Modeled spatial-temporal distribution
684 of productivity, chlorophyll, iron and nitrate on the northern Gulf of Alaska shelf relative
685 to field observations. *Deep-Sea Research Part II: Topical Studies in*
686 *Oceanography*, 165(April 2018), 163–191. https://doi.org/10.1016/j.dsr2.2019.05.006
687 Cross, J., Monacci, N., & Mathis, J. (2019). Dissolved inorganic carbon (DIC), total alkalinity
688 and other hydrographic and chemical variables collected from discrete samples and
689 profile observations during NOAA Ship Ronald H. Brown cruise RB1504 (EXPOCODE
690 33RO20150713) in the Gulf of Alaska from 2015-07-13 to 2015-07-31 [Data set].
691 Retrieved from https://catalog.data.gov/dataset/dissolved-inorganic-carbon-dic-total-
692 alkalinity-and-other-hydrographic-and-chemical-variables-c10
693 Crusius, J., Schroth, A. W., Resing, J. A., Cullen, J., & Campbell, R. W. (2017). Seasonal and
694 spatial variabilities in northern Gulf of Alaska surface water iron concentrations driven

by shelf sediment resuspension, glacial meltwater, a Yakutat eddy, and dust. *Global Biogeochemical Cycles*, *31*(6), 942–960. https://doi.org/10.1002/2016GB005493

Danielson, S. L., Hennon, T. D., Monson, D. H., Suryan, R. M., Campbell, R. W., Baird, S. J., et al. (2022). Temperature variations in the northern Gulf of Alaska across synoptic to century-long time scales. *Deep Sea Research Part II: Topical Studies in Oceanography*, *203*, 105155. https://doi.org/10.1016/j.dsr2.2022.105155

Desmet, F., Münnich, M., & Gruber, N. (2023). *Spatiotemporal heterogeneity in the increase of ocean acidity extremes in the Northeast Pacific* (preprint). Earth System Science/Response to Global Change: Climate Change. https://doi.org/10.5194/bg-2023-60

Di Lorenzo, E., Schneider, N., Cobb, K. M., Franks, P. J. S., Chhak, K., Miller, A. J., et al. (2008). North Pacific Gyre Oscillation links ocean climate and ecosystem change. *Geophysical Research Letters*, *35*(8), L08607. https://doi.org/10.1029/2007GL032838

Di Lorenzo, Emanuele, & Mantua, N. (2016). Multi-year persistence of the 2014/15 North Pacific marine heatwave. *Nature Climate Change*, *6*(11), 1042–1047. https://doi.org/10.1038/nclimate3082

Fisheries, N. (2023, January 4). Ecosystem Status Report 2022 Gulf of Alaska | NOAA Fisheries. Retrieved July 27, 2023, from https://www.fisheries.noaa.gov/resource/data/ecosystem-status-report-2022-gulf-alaska

Gaitán-Espitia, J. D., Marshall, D., Dupont, S., Bacigalupe, L. D., Bodrossy, L., & Hobday, A. J. (2017). Geographical gradients in selection can reveal genetic constraints for evolutionary responses to ocean acidification. *Biology Letters*, *13*(2), 20160784. https://doi.org/10.1098/rsbl.2016.0784

718 Gianguzza, P., Visconti, G., Gianguzza, F., Vizzini, S., Sarà, G., & Dupont, S. (2014).
719 Temperature modulates the response of the thermophilous sea urchin Arbacia lixula early
720 life stages to CO_2-driven acidification. *Marine Environmental Research*, *93*, 70–77.
721 https://doi.org/10.1016/j.marenvres.2013.07.008
722 Global Ocean Gridded L 4 Sea Surface Heights And Derived Variables Reprocessed 1993.
723 Ongoing. E.U. Copernicus Marine Service Information (CMEMS). Marine Data Store
724 (MDS). https://doi.org/10.48670/moi-00148 (Accessed on 01-08-2023)
725 Global Ocean Physics Analysis and Forecast. E.U. Copernicus Marine Service Information
726 (CMEMS). Marine Data Store (MDS). https://doi.org/10.48670/moi-00016 (Accessed on
727 09-08-2023)
728 Goethel, D.R., Rodgveller, C.J., Echave, K.B., Shotwell, S.K., Siwicke, K.A., Hanselman, D.
729 Malecha, P.W., Cheng, M., Williams, M., Omori, K., and Lunsford, C.R. (2022).
730 Assessment of the sablefish stock in Alaska. In Stock assessment and fishery evaluation
731 report for the groundfish resources of the Gulf of Alaska, North Pacific Fishery
732 Management Council, 1007 West Third, Suite 400, Anchorage, Alaska 99501.
733 Gruber, N., Boyd, P. W., Frölicher, T. L., & Vogt, M. (2021). Ocean Biogeochemical Extremes
734 and Compound Events. *Nature*, 395–407. https://doi.org/10.1038/s41586-021-03981-7
735 Hamon, M., Beuvier, J., Somot, S., Lellouche, J., Greiner, E., Arsouze, T., et al. (2016). Design
736 and validation of MEDRYS, a Mediterranean Sea reanalysis over the period 1992–2013.
737 *Ocean Science*, *2*, 577–599. https://doi.org/10.5194/os-12-577-2016
738 Hastings, K. K., Gelatt, T. S., Maniscalco, J. M., Jemison, L. A., Towell, R., Pendleton, G. W., &
739 Johnson, D. S. (2023). Reduced survival of Steller sea lions in the Gulf of Alaska

following marine heatwave. *Frontiers in Marine Science*, *10*. Retrieved from https://www.frontiersin.org/articles/10.3389/fmars.2023.1127013

Hauri, C., Schultz, C., Hedstrom, K., Danielson, S., Irving, B., Doney, S. C., et al. (2020). A regional hindcast model simulating ecosystem dynamics, inorganic carbon chemistry, and ocean acidification in the Gulf of Alaska. *Biogeosciences*, *17*(14), 3837–3857. https://doi.org/10.5194/bg-17-3837-2020

Hauri, C. & Irving, B. (2021). *Inorganic Carbon data from water samples collected during CTD casts at stations during the Northern Gulf of Alaska LTER seasonal cruises, 2018-2020*. ResearchWorkspace. 10.24431/rw1k45g, version: 10.24431_rw1k45g_20210525T174234Z.

Hauri, C., Pagès, R., McDonnell, A. M. P., Stuecker, M. F., Danielson, S. L., Hedstrom, K., et al. (2021). Modulation of ocean acidification by decadal climate variability in the Gulf of Alaska. *Communications Earth & Environment*, *2*(1), 1–7. https://doi.org/10.1038/s43247-021-00254-z

Hedstrom, K., Mack, S., Hadfield, M., and Hetland, R.: kshedstrom/roms: Master branch with COBALT early 2020 (Version v3.9_cobalt), Zenodo, https://doi.org/10.5281/zenodo.3647609, 2020

Hill, D. F., Bruhis, N., Calos, S. E., Arendt, A., & Beamer, J. (2015). Spatial and temporal variability of freshwater discharge into the Gulf of Alaska. *Journal of Geophysical Research: Oceans*, *120*(2), 634–646. https://doi.org/10.1002/2014JC010395

Hobday, A., Oliver, E., Sen Gupta, A., Benthuysen, J., Burrows, M., Donat, M., et al. (2018). Categorizing and Naming Marine Heatwaves. *Oceanography*, *31*(2), 162–173. https://doi.org/10.5670/oceanog.2018.205

764 Humphreys, M. P., Lewis, E. R., Sharp, J. D., & Pierrot, D. (2022). PyCO2SYS v1.8: marine
765 carbonate system calculations in Python. *Geoscientific Model Development*, *15*(1), 15–
766 43. https://doi.org/10.5194/gmd-15-15-2022
767 IOC-UNESCO (2022). Multiple Ocean Stressors: A Scientific Summary for Policy Makers. In
768 (Boyd PW, Dupont S & Isensee K, eds). Paris, UNESCO. 20 pp. (IOC Information
769 Series, 1404) doi:10.25607/OBP-1724.
770 Ladd, C., Stabeno, P., & Cokelet, E. D. (2005). A note on cross-shelf exchange in the northern
771 Gulf of Alaska. *Deep Sea Research Part II: Topical Studies in Oceanography*, *52*(5),
772 667–679. https://doi.org/10.1016/j.dsr2.2004.12.022
773 Lan, X., Tans, P., Thoning, K. W., & NOAA Global Monitoring Laboratory. (2023). NOAA
774 Greenhouse Gas Marine Boundary Layer Reference - CO2. [Data set].
775 https://doi.org/10.15138/DVNP-F961
776 Laufkötter, C., Zscheischler, J., & Frölicher, T. L. (2020). High-impact marine heatwaves
777 attributable to human-induced global warming. *Science*, *369*(6511), 1621–1625.
778 https://doi.org/10.1126/science.aba0690
779 Laurel, B. J., Abookire, A., Barbeaux, S. J., Almeida, L. Z., Copeman, L. A., Duffy-Anderson,
780 J., et al. (2023). Pacific cod in the Anthropocene: An early life history perspective under
781 changing thermal habitats. *Fish and Fisheries*, *00 (1-20)*.
782 https://doi.org/10.1111/faf.12779
783 Le Grix, N., Zscheischler, J., Laufkötter, C., Rousseaux, C. S., & Frölicher, T. L. (2021).
784 Compound high-temperature and low-chlorophyll extremes in the ocean over the satellite
785 period. *Biogeosciences*, *18*(6), 2119–2137. https://doi.org/10.5194/bg-18-2119-2021

Le Grix, N. (2021). Data used for creating the figures in "Compound high temperature and low chlorophyll extremes in the ocean over the satellite period" (Version 1), Zenodo, https://doi.org/10.5281/zenodo.4542015

Leonard, M., Westra, S., Phatak, A., Lambert, M., van den Hurk, B., Mcinnes, K., et al. (2014). A compound event framework for understanding extreme impacts. *Wiley Interdisciplinary Reviews: Climate Change*, *5*(1), 113–128. https://doi.org/10.1002/wcc.252

Lippiatt, S. M., Lohan, M. C., & Bruland, K. W. (2010). The distribution of reactive iron in northern Gulf of Alaska coastal waters. *Marine Chemistry*, *121*(1–4), 187–199. https://doi.org/10.1016/j.marchem.2010.04.007

Mantua, N. J., Hare, S. R., Zhang, Y., Wallace, J. M., & Francis, R. C. (1997). A Pacific Interdecadal Climate Oscillation with Impacts on Salmon Production. *Bulletin of the American Meteorological Society*, *78*(6), 1069–1079. https://doi.org/10.1175/1520-0477(1997)078<1069:APICOW>2.0.CO;2

Oliver, E. C. J., Burrows, M. T., Donat, M. G., Sen Gupta, A., Alexander, L. V., Perkins-Kirkpatrick, S. E., et al. (2019). Projected Marine Heatwaves in the 21st Century and the Potential for Ecological Impact. *Frontiers in Marine Science*, *6*, 734. https://doi.org/10.3389/fmars.2019.00734

Pages, R., Hedstrom, K., & Hauri, C. (2023). Configuration files for ROMS-COBALT used in Hauri et al., 2023: More than marine heatwaves: A new regime of heat, acidity, and low oxygen compound extreme events in the Gulf of Alaska. Zenodo. https://doi.org/10.5281/zenodo.8316392

Pages, R. (2023). Python scripts used in Hauri et al., 2023: More than marine heatwaves: A new regime of heat, acidity, and low oxygen compound extreme events in the Gulf of Alaska. Zenodo. 10.5281/zenodo.8291232

Pedregosa, F., Varoquaux, G., Gramfort, A., Michel, V., Thirion, B., Grisel, O., et al. (2011). Scikit-learn: Machine Learning in Python. *Journal of Machine Learning Research*, *12*(85), 2825–2830.

Perruche, C. (2019). Product User Manual for the Global Ocean Biogeochemistry Hindcast GLOBAL_REANALYSIS_BIO_001_029. Version.

Piatt, J. F., Parrish, J. K., Renner, H. M., Schoen, S. K., Jones, T. T., Arimitsu, M. L., et al. (2020). Extreme mortality and reproductive failure of common murres resulting from the northeast Pacific marine heatwave of 2014-2016. *PLOS ONE*, *15*(1), e0226087. https://doi.org/10.1371/journal.pone.0226087

Rodgers, K. B., Lee, S.-S., Rosenbloom, N., Timmermann, A., Danabasoglu, G., Deser, C., et al. (2021). Ubiquity of human-induced changes in climate variability. *Earth System Dynamics*, *12*(4), 1393–1411. https://doi.org/10.5194/esd-12-1393-2021

Rogers, L. A., Wilson, M. T., Duffy-Anderson, J. T., Kimmel, D. G., & Lamb, J. F. (2021). Pollock and “the Blob”: Impacts of a marine heatwave on walleye pollock early life stages. *Fisheries Oceanography*, *30*(2), 142–158. https://doi.org/10.1111/fog.12508

Sathyendranath, S., Stuart, V., Nair, A., Oka, K., Nakane, T., Bouman, H., et al. (2009). Carbon-to-chlorophyll ratio and growth rate of phytoplankton in the sea. *Marine Ecology Progress Series*, *383*, 73–84. https://doi.org/10.3354/meps07998

Sculley, D. (2010). Web-scale k-means clustering. In *Proceedings of the 19th international conference on World wide web* (pp. 1177–1178). Raleigh North Carolina USA: ACM. https://doi.org/10.1145/1772690.1772862

Shchepetkin, A. F., & McWilliams, J. C. (2005). The regional oceanic modeling system (ROMS): a split-explicit, free-surface, topography-following-coordinate oceanic model. *Ocean Modelling*, *9*(4), 347–404. https://doi.org/10.1016/j.ocemod.2004.08.002

Stabeno, P. J., Bell, S., Cheng, W., Danielson, S., Kachel, N. B., & Mordy, C. W. (2016). Long-term observations of Alaska Coastal Current in the northern Gulf of Alaska. *Deep Sea Research Part II: Topical Studies in Oceanography*, *132*, 24–40. https://doi.org/10.1016/j.dsr2.2015.12.016

Stock, C. A., Dunne, J. P., & John, J. G. (2014). Global-scale carbon and energy flows through the marine planktonic food web: An analysis with a coupled physical-biological model. *Progress in Oceanography*, *120*, 1–28. https://doi.org/10.1016/j.pocean.2013.07.001

Strom, S., Macri, E., & Fredrickson, K. (2010). Light limitation of summer primary production in the coastal Gulf of Alaska: physiological and environmental causes. *Marine Ecology Progress Series*, *402*, 45–57. https://doi.org/10.3354/meps08456

Strom, S., and the Northern Gulf of Alaska Long-Term Ecosystem Research Team. 2023. Recent marine heatwaves affect marine ecosystems from plankton to seabirds in the northern Gulf of Alaska. In Frontiers in Ocean Observing: Emerging Technologies for Understanding and Managing a Changing Ocean. E.S. Kappel, V. Cullen, M.J. Costello, L. Galgani, C. Gordó-Vilaseca, A. Govindarajan, S. Kouhi, C. Lavin, L. McCartin, J.D. Müller, B. Pirenne, T. Tanhua, Q. Zhao, and S. Zhao, eds, *Oceanography* 36(Supplement 1):31–33, https://doi.org/10.5670/oceanog.2023.s1.9.

852 Suryan, R. M., Arimitsu, M. L., Coletti, H. A., Hopcroft, R. R., Lindeberg, M. R., Barbeaux, S.
853 J., et al. (2021). Ecosystem response persists after a prolonged marine heatwave.
854 *Scientific Reports*, *11*(1), 6235. https://doi.org/10.1038/s41598-021-83818-5
855 Taylor, K. E. (2001). Summarizing multiple aspects of model performance in a single diagram.
856 *Journal of Geophysical Research: Atmospheres*, *106*, 7183–7192.
857 Thompson, P. L., Nephin, J., Davies, S. C., Park, A. E., Lyons, D. A., Rooper, C. N., et al.
858 (2023). Groundfish biodiversity change in northeastern Pacific waters under projected
859 warming and deoxygenation. *Philosophical Transactions of the Royal Society of London.*
860 *Series B, Biological Sciences*, *378*(1881), 20220191.
861 https://doi.org/10.1098/rstb.2022.0191
862 Thomsen, J., Casties, I., Pansch, C., Körtzinger, A., & Melzner, F. (2013). Food availability
863 outweighs ocean acidification effects in juvenile Mytilus edulis: laboratory and field
864 experiments. *Global Change Biology*, *19*(4), 1017–27. https://doi.org/10.1111/gcb.12109
865 Tsujino, H., Urakawa, S., Nakano, H., Small, R. J., Kim, W. M., Yeager, S. G., et al. (2018).
866 JRA-55 based surface dataset for driving ocean–sea-ice models (JRA55-do). *Ocean*
867 *Modelling*, *130*(December 2017), 79–139. https://doi.org/10.1016/j.ocemod.2018.07.002
868 Van Oostende, N., Dussin, R., Stock, C. A., Barton, A. D., Curchitser, E., Dunne, J. P., & Ward,
869 B. B. (2018). Simulating the ocean's chlorophyll dynamic range from coastal upwelling
870 to oligotrophy. *Progress in Oceanography*, *168*(August 2017), 232–247.
871 https://doi.org/10.1016/j.pocean.2018.10.009
872 Van Straalen, M. N. (2003). Peer Reviewed: Ecotoxicology Becomes Stress Ecology.
873 *Environmental Science & Technology*, *37*(17), 324A-330A.
874 https://doi.org/10.1021/es0325720

875 Vargas, C. A., Lagos, N. A., Lardies, M. A., Duarte, C., Manríquez, P. H., Aguilera, V. M., et al.
876 (2017). Species-specific responses to ocean acidification should account for local
877 adaptation and adaptive plasticity. *Nature Ecology & Evolution,* 1, 0084.
878 https://doi.org/10.1038/s41559-017-0084
879 Vargas, C. A., Cuevas, L. A., Broitman, B. R., San Martin, V. A., Lagos, N. A., Gaitán-Espitia,
880 J. D., & Dupont, S. (2022). Upper environmental pCO2 drives sensitivity to ocean
881 acidification in marine invertebrates. *Nature Climate Change*, *12*(2), 200–207.
882 https://doi.org/10.1038/s41558-021-01269-2
883 Von Biela, V. R., Arimitsu, M. L., Piatt, J. F., Heflin, B., Schoen, S. K., Trowbridge, J. L., &
884 Clawson, C. M. (2019). Extreme reduction in nutritional value of a key forage fish during
885 the pacific marine heatwave of 2014-2016. *Marine Ecology Progress Series*, *613*(May),
886 171–182. https://doi.org/10.3354/meps12891
887 Wanninkhof, Rik; Pierrot, Denis (2016): Underway physical oceanography and carbon dioxide
888 measurements during Ronald H. Brown cruise 33RO20150525. NOAA-Atlantic
889 Oceanographic and Meteorological Laboratory, Miami, PANGAEA,
890 https://doi.org/10.1594/PANGAEA.865900,
891 Ward, M., Kindinger, T., Hirsh, H., Ward, M., Hill, T., Jellison, B., Lummis, S. et al. (2022).
892 Reviews and syntheses: spatial and temporal patterns in metabolic fluxes inform potential
893 for seagrass to locally mitigate ocean acidification. *Biogeosciences,* 19, 689–699,
894 https://doi.org/10.5194/bg-19-689-2022
895 Weitzman, B., Konar, B., Iken, K., Coletti, H., Monson, D., Suryan, R., et al. (2021). Changes in
896 Rocky Intertidal Community Structure During a Marine Heatwave in the Northern Gulf

of Alaska. *Frontiers in Marine Science*, *8*.
https://doi.org/10.3389/fmars.2021.556820
Widdicombe, S., Isensee, K., Artioli, Y., Gaitán-Espitia, J. D., Hauri, C., Newton, J. A., et al. (2023). Unifying biological field observations to detect and compare ocean acidification impacts across marine species and ecosystems: what to monitor and why. *Ocean Science*, *19*(1), 101–119. https://doi.org/10.5194/os-19-101-2023
Yang, Q., Cokelet, E. D., Stabeno, P. J., Li, L., Hollowed, A. B., Palsson, W. A., et al. (2019). How "The Blob" affected groundfish distributions in the Gulf of Alaska. *Fisheries Oceanography*, *28*(4), 434–453. https://doi.org/10.1111/fog.12422

Tables

Table 1. Table showing the chlorophyll to carbon ratio (Chl/C) for each COBALT phytoplankton group as used in Hauri et al., (2020) and in the current model version. The Chl/C for the large phytoplankton was based on Gulf of Alaska *in situ* values(Strom et al., 2010; Coyle et al., 2019). Chl/C for medium was reduced by the same amount (28%) as large phytoplankton to remain smaller and is now at the higher range of the value given by (Sathyendranath et al., (2009). Chl/C for small phytoplankton and diazotrophs was reduced to what was found by Sathyendranath et al. (2009).

Phytoplankton group	Chl/C (Hauri et al., 2020)	Chl/C This version
Large	0.07	0.05
Medium	0.05	0.035

Small	0.03	0.008
Diazotroph	0.03	0.008

915

916